JOURNAL OF MATERIALS SCIENCE 8 (1973) 793–806

High-strength graphite fibre/lithium aluminosilicate composites

S. R. LEVITT*
Ferro Corporation, Technical Center, Independence, Ohio, USA

Graphite fibre/lithium aluminosilicate composites of matrix composition $Li_2O\ Al_2O_3 \cdot nSiO_2$ where $n = 3$, 4, and 8, have been developed with a high volume fraction of undirectionally aligned graphite fibres. Graphite fibre/ceramic matrix tapes were produced on a drum-winding apparatus and hot-pressed to final dimensions. This composite system exhibits a combination of useful properties, including high strength, low density, excellent thermal shock resistance and impact strength. Shear strength, cyclic modulus of rupture and modulus of elasticity and optical and electron microscopic evaluation of microstructure are discussed. Modulus of rupture as a function of vol % fibres was studied. The high modulus of rupture and impact strength are discussed in terms of the relative properties of fibre and matrix.

1. Introduction

For ceramics to find greater applicability as engineering materials, major improvements in strength and toughness, ie, resistance to thermal and mechanical shock, are needed. Ceramic materials are generally considered "brittle" with low work of fracture due to the relative ease of crack propagation. Recent studies have shown that one promising approach to this problem is the design of fibre-reinforced ceramic matrix composites [1-3]. Matrix deformation allows stress transfer to the reinforcing fibres by means of shear or frictional forces at the fibre-matrix interface. Fibres of sufficient length with higher tensile strength and elastic modulus than the matrix, will produce effective matrix reinforcement and also may help retard crack propagation, producing increased toughness.

High strength fibres are not useful structural materials until they are bonded together by a suitable matrix material. To achieve maximum directional properties, the fibres must be oriented parallel to produce unidirectional fibre alignment. For maximum strength the overall system must be designed so that the fibres carry the major part of the applied load, while the matrix binds the fibres together, spaces them, protects them from mechanical and chemical damage and distributes the load to the individual fibres. Effective load distribution occurs when fibres of high modulus of elasticity are embedded in a matrix of much lower modulus. Maximum attainable composite strength elastic modulus can be predicted from the rules of mixtures [4]. For example, the tensile strength of a fibre-reinforced composite with continuous and parallel fibres is given by:

$$S_c = S_m^* (1 - V_f) + S_f V_f,\ V_f > V_m$$

where S_c = ultimate tensile stress of the composite, S_m^* = tensile stress on matrix when composite is strained to its S_c, S_f = ultimate tensile stress of fibres, V_f = volume fraction of fibres.

A similar relation exists for modulus of elasticity [4]. As the volume fraction of fibres increases, the per cent load assumed by the fibres also increases. As the ratio E fibre/E matrix increases, a greater fraction of the total load will be carried by the fibres, so that increasing E_f/E_m allows the use of a smaller vol % fibre to carry a given fraction of applied load. In practice, actual mechanical properties may deviate significantly from theoretical values due to fibre-matrix bonding effects, interfacial interaction, oxidation, matrix cracking, porosity, inherent defects and impurities in the fibres, fibre orientation, fibre damage inherent in high

*Presently attending Case Western Reserve University, School of Medicine, Cleveland, Ohio 44106.

temperature–high pressure processing techniques and thermal expansion mismatch between fibre and matrix.

No significant strength increases have been obtained in many ceramic composite systems owing to matrix-reinforcement reaction at processing or projected use temperatures, as well as deleterious expansion-coefficient incompatibility in chemically stable combinations [5, 6]. However, some success in overcoming these difficulties has been reported [7].

During the present study, it has been found that the graphite fibre/lithium aluminosilicate system appears to be one in which many of the above problems are overcome*. Substantial increases in strength over the unreinforced ceramic matrix have been obtained. This is attributed to the relative thermal expansion behaviour of fibre and matrix, a large mismatch in modulus of elasticity and strength between fibre and matrix, and the formation of a fibre-matrix bond. A method has been developed for fabricating ceramic composites containing a high volume fraction of unidirectionally aligned graphite fibres in a continuous and dense lithium aluminosilicate matrix. The method is based on the formation of a graphite fibre-ceramic matrix tape with subsequent hot-pressing to form the final body. Resulting composites exhibit flexural strengths greater than 100000 psi at room temperature, low density, and excellent thermal shock resistance and impact strength.

2. Experimental procedure

2.1. Preparation of materials

Reagent lithium carbonate, A-14 alumina (−325 mesh) and powdered quartz (−400 mesh) were mixed in proper proportions to give $Li_2O{\cdot}Al_2O_3{\cdot}nSiO_2$, where $n = 3$, 4, and 8. Carbowax binder was added (3%) and 5 in. × 10 in. (12.5 cm × 25 cm) slabs were pressed under 1000† psi and fired at 1300°C for 4 h, then crushed and dry ball milled for 10 h and screened through −200 mesh sieves. To obtain complete reaction, this procedure was repeated with a final wet ball milling in Synasol for 16 h. X-ray diffraction results indicated the presence of β-eucryptite-silica solid solution ($Li_2O{\cdot}Al_2O_3{\cdot}3SiO_2$), β-spodumene ($Li_2O{\cdot}Al_2O_3{\cdot}4SiO_2$) and β-spodumene-silica solid solution ($Li_2O{\cdot}Al_2O_3{\cdot}8SiO_2$).

*Patent applied for.
†1000 psi = 6.895 × 10^6 Nm^{-2}.

Hercules HM-S continuous graphite tows have been used with manufacturer's property specifications given in Table I. The tow consists of a continuous strand of fibres containing 10000 filaments, each filament 8 μm in diameter.

TABLE I Properties of Hercules HM-S continuous graphite tows

Ultimate tensile strength (10^3 psi, 6.895 × 10^6 N m^{-2})	250-350
Modulus of elasticity (10^6 psi, 6.895 × 10^9 Nm^{-2})	50-60
Density (g cm^{-3})	1.91
Treatment	Surface-treated

2.2. Composite fabrication

A schematic diagram of the drum winding operation to produce graphite fibre ceramic tape is shown in Fig. 1. The continuous graphite tow is removed from a spool, impregnated with slip and directed onto a rotating drum at 5¼ tows per in. (~2 tows per cm). The drum is covered with a Teflon-impregnated glass fabric to avoid sticking and allow easy removal of the dried tape. A Teflon squeegee traverses the drum as the tape is wound, removing excess slip from the tape surface. The slip consisted of powdered ceramic of appropriate particle size, a 3% polyvinyl alcohol/water binder and triethylene glycol as plasticizer. The slip composition can be used to control the relative percentages of fibre and matrix in the final composite. The tape is dried, removed from the drum and cut into 2 in. × 2 in. (5 cm × 5 cm) squares which are layed up to give undirectional fibre alignment, and then hot-pressed.

Both composites and unreinforced bodies are hot pressed in graphite moulds to produce 2 in. × 2 in. (5 cm × 5 cm) coupons of various thicknesses, Fig. 2. Hot-pressing is performed under a N_2 atmosphere and all graphite parts are coated with colloidal graphite (Aquadag) to further reduce oxidation. In addition, a 0.003 in (0.08 mm) molybdenum foil is used as a die liner to prevent reactions with the mould walls, facilitate pellet release and extend mould life. Hot-pressing temperatures are obtained in 25 to 35 min and held for 5 min during application of 1000 psi. Pressure is applied and held constant by using pressurized gas on a hydraulic ram and temperature is measured using a Pt-Pt 10% Rh thermocouple.

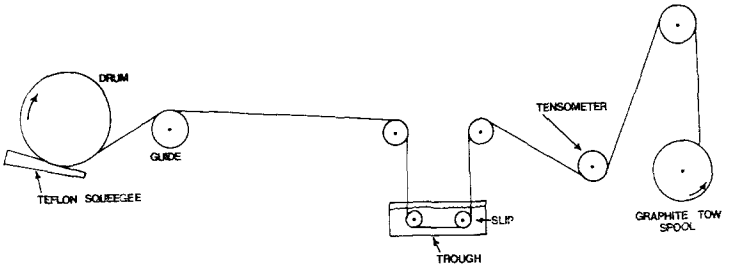

Figure 1 Drum winding process to produce graphite/ceramic tape.

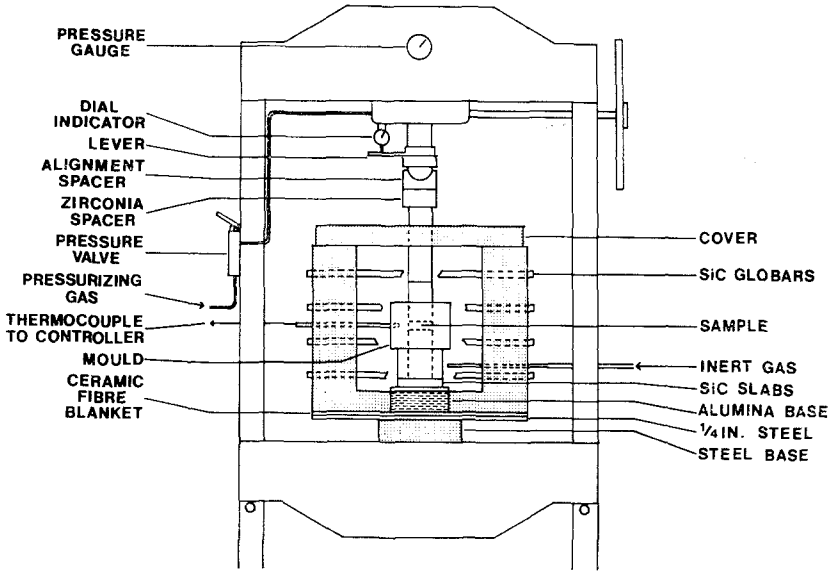

Figure 2 Schematic drawing of hot-press.

2.3. Sample preparation

Test bars were cut from 2 in. × 2 in. hot-pressed pellets using a diamond saw and ground to final dimensions by hand using a number 240 diamond impregnated wheel. Polished sections were prepared for reflected light observation using a Nomarski interference microscope. Samples were encased in epoxy resin and then ground and polished starting with a 240-grit bonded diamond lap, then a 30 μm bonded diamond lap and finally 6 to 12, 1 to 5 and 1 μm diamond paste. Two stage carbon-platinum replicas were prepared from polished sections and fracture surfaces for electron microscopy. Concentrated HF fumes were used as etchant.

2.4. Physical and mechanical properties

Bulk density was determined on test bars by the water immersion method [8]. Density determinations by weighing and measuring dimensions produced no significant deviations attributable to water absorption into open pores. Wt % fibres was determined from the weight change after oxidizing the powdered composites to constant weight in air at 1000° C. Vol % fibres was calculated from wt % fibres, fibre density and composite density. Flexural test specimens were approximately 2 in. × $\frac{1}{4}$ in. × $\frac{1}{20}$ in. (5.1 cm × 0.64 cm × 0.13 cm) with specimen length parallel to the fibre axis. Load versus crosshead travel was measured in three-point bending on a universal testing machine* using $\frac{1}{8}$ in. (0.317 cm) diameter sapphire loading pins at a span of 1.50 in. (3.81 cm). The loading rate was 0.05 in. min^{-1} (0.13 cm min^{-1}); corrections were made for machine compliance and the

*Instron Corporation, Canton, Mass.

modulus of rupture and modulus of elasticity were calculated. A span/depth ratio of about 30/1 is used to minimize shear and wedging effects and obtain tensile fracture modes in three-point bending. Short beam shear specimens were approximately 1 in. × ¼ in. × ⅛ in. (2.54 cm × 0.64 cm × 0.317 cm) with length parallel to the fibre axis. Tests were made under three-point loading using ¼ in. (0.64 cm) diameter steel loading pins at a variable span/depth ratio and loading rate of 0.05 in. min^{-1} (0.13 cm min^{-1}). Notched and unnotched Izod impact samples have been prepared and tested according to ASTM D-256 using a pendulum type impact tester*. Sample geometries are shown in Fig. 3. Modulus of rupture was measured before and after rapid thermal cycling between room temperature and 1200°C. Flexural specimens were placed in a refractory tube purged with nitrogen, which is then inserted into a furnace preheated to 1200°C. After a 5-min soak, the test bars were quenched in water and then recycled or tested.

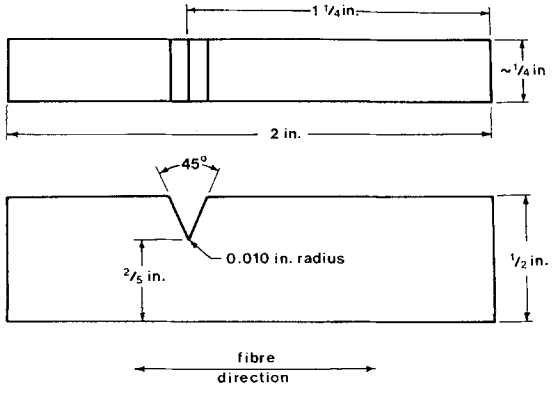

Figure 3 Notched izod impact test specimen.

3. Results and discussion

A graphite fibre reinforcing phase in a lithium-aluminosilicate matrix was chosen for study based on their relative properties. The particular graphite fibres employed have high tensile strength, elastic modulus and radial thermal expansion coefficient and low axial thermal expansion coefficient. The lithium-aluminosilicates have relatively low tensile strengths and elastic moduli and low thermal expansion coefficients. Such a mismatch in properties was thought to be important for the fibres to be effectively utilized as a reinforcing phase.

3.1. Graphite fibre /$Li_2O{\cdot}Al_2O_3{\cdot}8SiO_2$

The first series of experiments was conducted using $Li_2O{\cdot}Al_2O_3{\cdot}8SiO_2$ as the ceramic matrix, with particle size distribution given in Table II. Hot-pressing was performed at 1375°C for 5 min under 1000 psi. A plot of modulus of rupture versus fibre vol % indicates that a "rule of mixtures" relationship is *apparently* being followed and the strengthening potential of the fibres is being very efficiently utilized (Fig. 4). Data scatter (Table III) indicates that the variability of these composites is substantially lower than that for conventional ceramics. Subsequent experiments have revealed that the modulus of rupture will vary for a given vol % fibre, depending on processing conditions and resulting pore volume, size and distribution, uniformity of fibre distribution, particle size distribution, etc.

TABLE II Particle size analysis for $Li_2O{\cdot}Al_2O_3{\cdot}8SiO_2$

Particle size (μm)	% between
20-10	9.2
10-7	14.6
7-4	21.8
4-1	47.0
1-0.6	4.6
0.6-0.2	2.8

As vol % fibres increased much above 36%, an increasing amount of porosity occurred in the composites and the modulus of rupture values declined. This problem may be minimized by proper adjustment of the particle size and slip viscosity (% PVA/H_2O solution) since at low percentages of ceramic in the slip, the increased slip fluidity allowed it to run off the tape during tape winding. An optimum slip composition based on the present results contained 40% ceramic and resulted in approximately 35 vol % fibres in the final composite, Table IV. This slip composition has been used in all subsequent studies. Composites of this composition with 25 to 35 vol % fibres can be successfully fabricated by hot-pressing for 5 min under 1000 psi at 1375°C. Property degradation occurred at higher pressure (4000 psi) due to fibre damage and at lower pressure (300 psi) due to a lack of

*Testing Machines Inc, Amityville, New York.

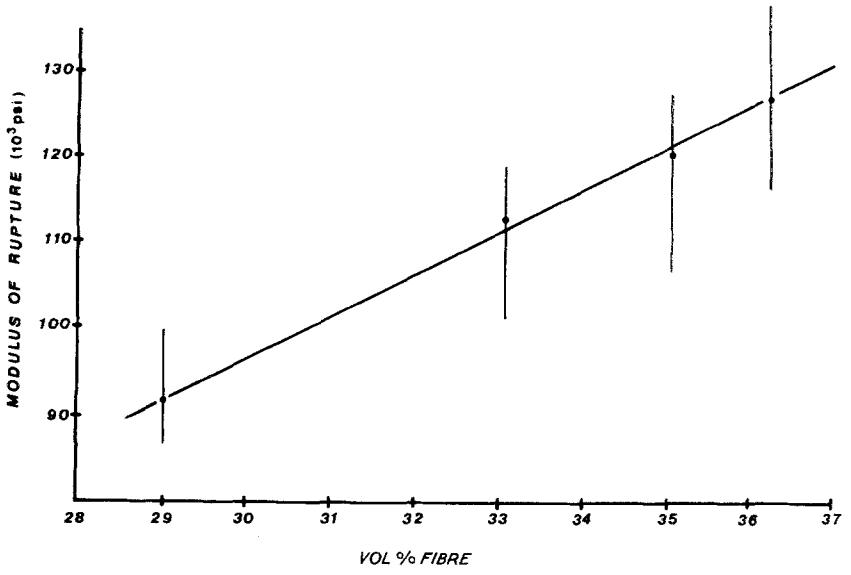

Figure 4 modulus of rupture versus fibre vol % for HM-S graphite/$Li_2O{\cdot}Al_2O_3{\cdot}8SiO_2$ composites.

TABLE III Properties of HM-S graphite fibre/$Li_2O{\cdot}Al_2O_3{\cdot}8SiO_2$ composites fabricated at 1375°C under 1000 psi for 5 min

Vol % fibres	Bulk density (g cm^{-3})	Modulus of rupture (psi)*	Average modulus of rupture (psi)	Standard deviation (psi)	Coefficient of variation
2.90	2.19	92400	91800	5400	5.9
		93000			
		99900			
		87100			
		86600			
33.1	2.16	101300	113400	7000	6.2
		115900			
		119100			
		117000			
		113900			
35.1	2.17	122600	120900	8400	7.0
		127400			
		120500			
		107000			
		127600			
36.3	2.15	116700	127400	7400	5.8
		121700			
		130000			
		138000			
		129500			
		128500			

*1000 psi = 6.895×10^6 Nm^{-2}.

densification and intimate fibre-matrix contact. Temperatures of 1400°C and higher produced excessive melting and temperatures of 1350°C produced a highly porous body. The highest strengths and most homogeneous microstructures were observed after hot-pressing at 1375°C.

TABLE IV Slip composition producing maximum flexural strength

	wt %
Ceramic matrix material ($Li_2O{\cdot}Al_2O_3{\cdot}8SiO_2$)	40
3% polyvinyl alcohol/water solution	58
Triethylene glycol	2

3.1.1. Microstructure

Optical micrographs (Fig. 5) show a typical composite microstructure with a relatively uniform fibre distribution and demonstrate the feasibility of incorporating a high volume fraction of fibres into this ceramic matrix. There is some degree of fibre twisting and misalignment in the composites, resulting in lower directional properties. In addition, scatter in individual fibre properties produced composite data scatter. Uniform fibre distribution is important and fibre-fibre contact should be avoided

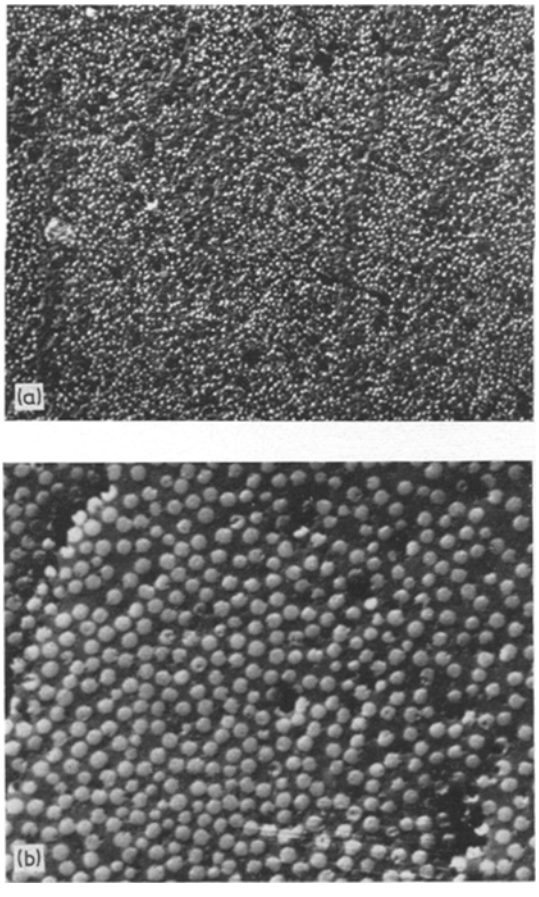

Figure 5 Polished sections of typical HM-S graphite/$Li_2O{\cdot}Al_2O_3{\cdot}8SiO_2$ composites; (a) ×76, (b) ×303.

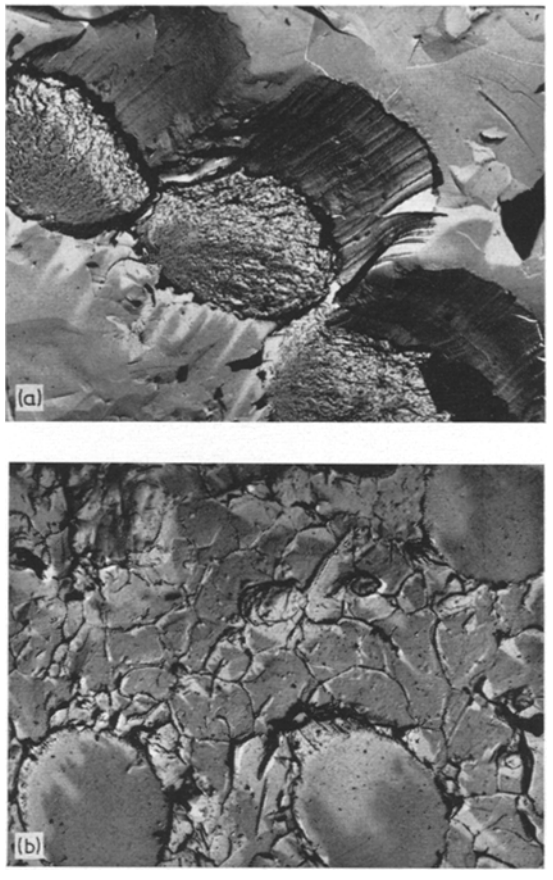

Figure 6 Electron micrographs of HM-S graphite/$Li_2O{\cdot}Al_2O_3{\cdot}8SiO_2$ composites. (a) Fracture surface, ×5040, (b) polished and etched, ×2500.

to eliminate local stress concentrations at points of contact. This would result in premature fibre failure, with cracks travelling through the composite by way of fibre-fibre contact points.

Electron microscope studies (Fig. 6) reveal a non-cracked matrix, indicating a satisfactory thermal expansion match between fibres and matrix. The appearance of the electron micrographs is an artifact produced by the replication technique and is not due to plastic deformation of the graphite fibres. Extremely intimate fibre-matrix contact was produced without any detectable interfacial reactions or degradation of fibre surface topography. Test bars broken in three-point bending exhibited crack deflection and fibre pull-out, with the crack propagating through the composite. Cracks were deflected to propagate parallel to the fibre axis with an undulating fracture surface running obliquely

through the composite. A hot-pressing temperature of 1375°C was found necessary to produce dense bodies with intimate fibre-matrix contact. This is 19°C above the reported melting point of the ceramic matrix [9, 10]. Partial melting of the ceramic during the rapid (5 min at 1375°C) hot-pressing cycle led to rapid densification and excellent fibre-matrix contact. The glass formed is highly viscous and allowed little recrystallization during the cooling cycle (about 2 h), as shown by X-ray diffraction. The residual glass did not appear to produce matrix cracking due to thermal expansion mismatch or to prevent the development of extremely high flexural strengths. The residual glass limits the high-temperature properties [11], but should be minimized by controlled recrystallization or eliminated entirely by pressure calcintering. Oxidation of the graphite fibres also limits elevated temperature properties in air [12].

3.1.2. *Directional properties, thermal shock, shear and cycling*

The flexural strength and flexural modulus were tested both parallel and perpendicular to the hot-pressing direction (both normal to the fibre direction) to emphasize the effects of pressure, laminations and non-uniform microstructure due to the various processing operations. The results (Table V) indicate little deviation in average flexural strength (about 4% from mean) or in average flexural modulus (about 5% from mean) when tested parallel or perpendicular to the hot-pressing direction. Thus, the microstructure and resulting properties do not appear to have substantial directional characteristics (about the fibre axis) with respect to hot-pressing direction.

Initial thermal shock tests have been conducted on these composites. There is presently no indication of flexural strength degradation after five thermal shock cycles between room temperature and 1200°C, Table VI. The low thermal expansion coefficients of fibre and matrix and high thermal conductivity of graphite fibre contribute to the thermal shock resistance.

The shear strength of typical graphite fibre/$Li_2O{\cdot}Al_2O_3{\cdot}8SiO_2$ composites is given in Table VII. The average modulus of rupture of these test bars is 126×10^3 psi (8.69×10^8 Nm^{-2}) (span/depth = 30/1). Span/depth ratios of 4/1 and 5/1 produced combination failure modes with the predominant mode being crushing. The accompanying tensile failure indications

TABLE V Properties of HM-S graphite/$Li_2O{\cdot}Al_2O_3{\cdot}8SiO_2$ composites tested parallel and perpendicular to hot-pressing direction

Test direction	Vol. % fibres	Bulk density (g cm^{-3})	Modulus of rupture (psi)*	Average modulus of rupture (psi)	Standard deviation (psi)	Coefficient of variation	Modulus of elasticity (10^6 psi)	Average modulus of elasticity (10^6 psi)	Standard deviation (10^6 psi)	Coefficient of variation
Perpendicular to hot press direction	39.6	2.06	116700	115800	8200	7.1	21.2	20.9	1.7	8.1
			109700				21.6			
			112800				20.7			
			111200				17.9			
			104700				19.5			
			129500				22.2			
			120700				22.9			
Parallel to hot press direction	39.6	2.06	121500	124800	5900	4.7	23.0	23.0	0.7	3.1
			130200				22.5			
			118200				22.0			
			127200				23.2			
			132300				24.1			
			119600				23.0			

*1000 psi = 6.895×10^6 Nm^{-2}.

TABLE VI Modulus of rupture versus thermal shock cycles between room temperature and 1200°C for graphite fibre/$Li_2O{\cdot}Al_2O_3{\cdot}8SiO_2$ composites

Thermal shock cycles	Modulus of rupture (psi)*	Average modulus of rupture (psi)
0	138000	124400
	121800	
	113400	
1	130200	129600
	129000	
5	121600	125000
	128400	

*1000 psi = 6.895×10^6 Nm^{-2}.

resulted from distortion in stress distribution produced by crushing. A span/depth ratio of 6/1 eliminated both crushing and the resulting tensile failure, and pure shear failures resulted, as determined microscopically. The average shear strength is about 5900 psi (4.1×10^7 Nm^{-2}).

A slight bend in the load versus deflection curves has been indicated between 30 and 50% of the failure load in many composites (Fig. 7). Three graphite fibre $Li_2O{\cdot}Al_2O_3{\cdot}8SiO_2$ composites have been cycled ten times in three-point loading (span/depth: 30/1) at room temperature to over 85000 psi (5.5×10^8 Nm^{-2}) and then loaded to failure on the eleventh cycle. The slight bend in the load versus deflection curve disappeared after the first cycle and from cycles 2 to 10 the load versus deflection curve appeared as a stabilized hysteresis. The slope of the load versus deflection curve on cycles 2 to 10 approached that above the bend on the first cycle. This produced a decrease in modulus of elasticity of about 6% after the first cycle, with no further decrease up to 10 cycles (Table VIII). The test bars were loaded to failure on the eleventh cycle and modulus of rupture values were as expected (Table VIII). Another small bend appeared on the eleventh cycle, just above the cycling load in the load versus deflection curve. A small amount of irreversible damage occurred during the first cycle above a critical load with none thereafter. This may result from a small number of poorly bonded or short fibres which fracture before the rest, fibre misalignment and/or matrix cracking after its critical strain is exceeded. Tensile strength variations in the individual graphite fibres could also cause such an effect.

3.1.3. Impact strength

The impact energy has been measured on Her-

TABLE VII Short-beam shear strength of HM-S graphite fibre/$Li_2O{\cdot}Al_2O_3{\cdot}8SiO_2$ composites hot-pressed at 1375°C under 1000 psi for 5 min

Short-beam shear stress (psi)*	Span/depth ratio	Failure mode
7300	4/1	Shear, tension, compression
6800	5/1	Shear, tension, compression
6200	6/1	Shear
5800	6/1	Shear
5800	6/1	Shear
6450	6/1	Shear
5400	6/1	Shear

*1000 psi = 6.895×10^6 Nm^{-2}.

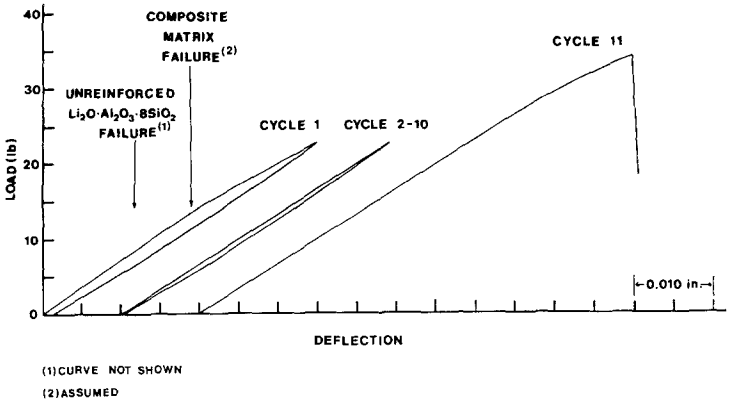

Figure 7 Cyclic testing of HM-S graphite/$Li_2O{\cdot}Al_2O_3{\cdot}8SiO_2$ composites.

TABLE VIII Cyclic flexural testing of HM-S graphite/$Li_2O{\cdot}Al_2O_3{\cdot}8SiO_2$ composites*

Cycle no.	Average stress (10^3 psi)	Average modulus of elasticity (10^6 psi)
1	87.9	20.9
2-10	87.9	19.7
11	126.7	19.7

*Hot-pressed at 1375°C for 5 min under 1000 psi (6.895×10^6 Nm^{-2}) 32.2 vol % fibre and bulk density = 2.17 g cm^{-3}).

cules HM-S graphite/$Li_2O{\cdot}Al_2O_3{\cdot}8SiO_2$ composites. Test samples were fabricated in the usual way and hot-pressed at 1375°C for 5 min under 1000 psi. Two nickel-base superalloys, Udimet 700 and MAR-M200†, used in turbine-blade applications and dense alumina‡, were tested under identical conditions. The composite impact energy for notched bars falls in the approximate range of 20 to 30 ft lb in^{-2} (4.2×10^4 to 6.3×10^4 Jm^{-2}) of cross section while that for unnotched test bars is about 75 ft lb in^{-2}, (1.6×10^5 Jm^{-2}), (Table IX). These values are extremely high for a ceramic material, as can be seen by comparison with an excellent quality alumina. Fig. 8 shows the macroscopic nature of the impact fracture on a notched composite test bar. The fracture is repeatedly deflected as it propagates across the test bar to produce a saw-tooth effect accompanied by fibre pull-out. Exposed fibres show little matrix adherence implying weak interfacial bonding. Fibre surface topography appears unaltered from unprocessed fibres with microscopic fluting running parallel to the fibre axis, Fig. 9.

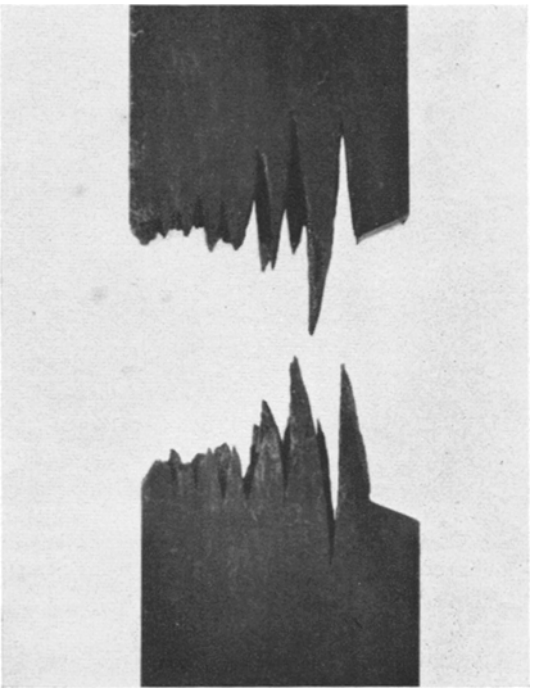

Figure 8 Notched izod impact failure of an HM-S graphite/$Li_2O{\cdot}Al_2O_3{\cdot}8SiO_2$ composite.

3.2. Compositional effects on properties

3.2.1. Modulus of rupture and modulus of elasticity

A series of experiments were conducted to determine the relative modulus of rupture and modulus of elasticity for both unreinforced bodies and HM-S graphite/lithium aluminosilicate composites of matrix composition $Li_2O{\cdot}Al_2O_3{\cdot}nSiO_2$ where n = 3, 4, and 8. These matrix compositions were synthesized as des-

TABLE IX Izod impact energy of HM-S graphite/$Li.O{\cdot}Al_2O_3{\cdot}8SiO_2$ composites, Udimet 700, MAR-M200 and alumina

Composition	No. test bar	Density (g cm^{-3})	Vol. % fibre	Notched	Impact energy (ft lb in^{-2})*
HM-S graphite fibre/$Li_2O.Al_2O_3.8SiO_2$ composites	2	2.19	31.6	no	75.5
	1	2.19	31.6	yes	28.3
	3	2.18	34.2	yes	20.0
	3	2.18	34.4	yes	22.3
U-700	2	—	—	yes	163.4
MAR-M200	3	—	—	yes	90.0
Al_2O_3 AP 35	3	—	—	yes	1.50
	2	—	—	no	3.34

*1 ft-lb $in^{-2} \equiv 2.100 \times 10^3$ Jm^{-2}.

†J. W. Sawyer, "Gas Turbine Engineering Handbook", 1st edn (Gas Turbine Publications, Samford, Conn, 9166) pp. 228.
‡AP35, McDanel Refractory Porcelain Co, Beaver Falls, Pa, Bulletin No. D866.

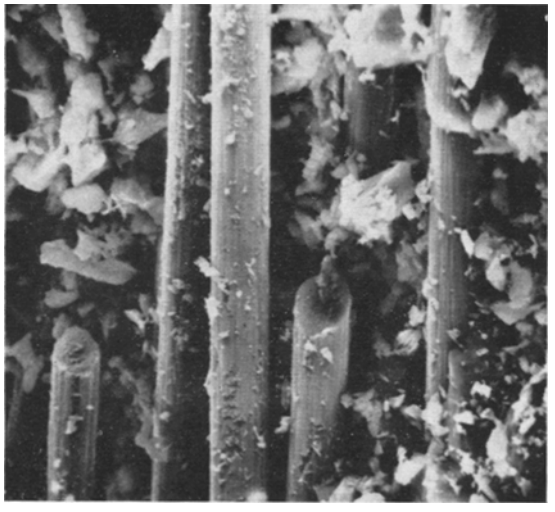

Figure 9 Scanning electron micrograph of izod impact fracture surface of HM-S graphite/$Li_2O{\cdot}Al_2O_3{\cdot}8SiO_2$ composite (×1000).

cribed above with particle size given in Table X. Experiments were conducted to determine the optimum hot pressing temperatures to obtain high density composites. These temperatures were always at or above the melting points of the ceramic matrices. For unreinforced bodies, hot-pressing temperatures as close as possible to those for related composites were used, the limiting factor being massive flow and extrusion from the mould due to melting.

The properties of hot-pressed unreinforced lithium aluminosilicates $Li_2O{\cdot}Al_2O_3{\cdot}nSiO_2$ where $n = 3$, 4, and 8 are given in Table XI. The modulus of rupture tended to increase as the silica content of the various compositions decreased. The densities of hot-pressed $Li_2O{\cdot}Al_2O_3{\cdot}nSiO_2$ where $n = 4$ and 8 were almost theoretical, indicating low porosity. The relative low hot-pressed density of $Li_2O{\cdot}Al_2O_3{\cdot}3SiO_2$ is indicative of porosity, which was borne out by optical microscopic examination of polished sections. The modulus of rupture of $Li_2O{\cdot}Al_2O_3{\cdot}3SiO_2$ would be expected to increase as theoretical density is approached. The elastic modulus increased on going from $Li_2O{\cdot}Al_2O_3{\cdot}8SiO_2$ to $Li_2O{\cdot}Al_2O_3{\cdot}4SiO_2$ but declined for $Li_2O{\cdot}Al_2O_3{\cdot}3SiO_2$. The presence of porosity also explains the relatively low value of elastic modulus for $Li_2O{\cdot}Al_2O_3{\cdot}3SiO_2$. The modulus of rupture and modulus of elasticity were determined using the same span/depth ratios as for composites (about 30/1). These values may now be compared to those of graphite fibre reinforced composites to determine the magnitude of property changes.

Composites were fabricated using the slip composition which produced maximum flexural strengths in previous work, Table IV. Substantial increases in both modulus of rupture and modulus of elasticity were found using all three matrix compositions (Table XII). The $Li_2O{\cdot}Al_2O_3{\cdot}8SiO_2$ matrix produced substantially higher modulus of rupture values than either of the other two matrix compositions.

3.2.2. Interpretation of results

The composites consist of graphite fibres having considerable anisotropy, embedded in a matrix containing the original crystalline phase, a glass phase formed during hot-pressing and a β-eucryptite-like phase formed by recrystallization from the glass phase. Both original and recrystallized crystalline phases are anisotropic with respect to thermal expansion coefficient, and may be randomly oriented. Some insight into the mechanism responsible for composite properties may be obtained by considering a simplified model consisting of the graphite fibres embedded in a homogeneous, isotropic polycrystalline matrix of the original crystalline composition and having a thermal expansion coefficient identical to that found for the polycrystalline body.

The coefficient of thermal expansion is $-10 \times 10^{-7}\,^{\circ}C^{-1}$ for $Li_2O{\cdot}Al_2O_3{\cdot}3SiO_2$, $10 \times 10^{-7}\,^{\circ}C^{-1}$ for $Li_2O{\cdot}Al_2O_3{\cdot}4SiO_2$ and $2 \times 10^{-7}\,^{\circ}C^{-1}$ for $Li_2O{\cdot}Al_2O_3{\cdot}8SiO_2$, measured on polycrystalline bodies from room temperature to 1000° C [14]. The graphite fibre is polycrystalline

TABLE X Particle size analysis for $Li_2O{\cdot}Al_2O_3{\cdot}nSiO_2$ where $n = 3$, 4 and 8

Particle size (μm)	% between for $Li_2O{\cdot}Al_2O_3{\cdot}3SiO_2$	% between for $Li_2O{\cdot}Al_2O_3{\cdot}4SiO_2$	% between for $Li_2O{\cdot}Al_2O_3{\cdot}8SiO_2$
10-7	2.5	10.3	11.9
7-4	9.8	12.3	15.1
4-1	76.4	65.8	64.9
1-0.6	11.3	11.6	8.1

TABLE XI Physical properties of hot-pressed lithium aluminosilicates

Composition	Hot-pressing temperature (°C)*	Density (g cm^{-3})	Modulus of rupture (psi)	Average modulus of rupture (psi)	Standard deviation (psi)	Coefficient of variation	Modulus of elasticity (10^6 psi)	Average modulus of elasticity (10^6 psi)	Standard deviation (10^6 psi)	Coefficient of variation
$Li_2O{\cdot}Al_2O_3{\cdot}3SiO_2$	1385	2.08	15800	15200	2000	12.9	11.3	11.1	1.2	10.7
			12000				9.3			
			15500				10.2			
			14000				12.1			
			17700				11.2			
			16000				12.5			
$Li_2O{\cdot}Al_2O_3{\cdot}4SiO_2$	1410	2.39	15300	15100	1100	7.5	11.4	11.6	1.3	11.0
			14700				12.8			
			16300				11.8			
			14500				11.7			
			16500				12.5			
			13500				9.2			
$Li_2O{\cdot}Al_2O{\cdot}8SiO_2$	1350	2.39	11800	12300	1000	8.3	8.5	10.1	1.0	10.2
			11500				9.9			
			13900				10.2			
			12800				10.9			
			11600				11.1			

*All compositions hot pressed for 5 min under 1000 psi (6.895×10^6 Nm^{-2}.)

TABLE XII Physical properties of HM-S graphite/$Li_2O{\cdot}Al_2O_3{\cdot}nSiO_2$ composites where n = 3, 4 and 8

Composition	Hot-pressing temperature	Vol % fibres	Density (g cm^{-3})	Modulus of rupture (psi)	Average modulus of rupture (psi)	Standard deviation (psi)	Coefficient of variation	Modulus of elasticity (10^6 psi)	Average modulus of elasticity (10^6 psi)	Standard deviation (10^6 psi)	Coefficient of variation
$Li_2O{\cdot}Al_2O_3{\cdot}3SiO_2$	1400	37.5	2.11	65500	59400	6500	10.9	22.0	21.5	1.0	4.5
				62800				20.3			
				66500				21.5			
				53800				20.5			
				48400				23.2			
				59400				21.7			
				59200				21.2			
$Li_2O{\cdot}Al_2O_3{\cdot}4SiO_2$	1425	41.0	2.15	58500	73300	8300	11.3	20.6	21.6	0.9	4.3
				79400				22.3			
				67000				21.7			
				77800				20.5			
				82800				22.9			
				72200				21.0			
				75700				22.3			
$Li_2O{\cdot}Al_2O{\cdot}8SiO_2$	1375	32.3	2.18	131500	125600	6700	5.4	21.7	21.3	0.6	2.9
				119000				20.6			
				135500				21.4			
				129400				22.0			
				120500				20.7			
				118300				20.6			
				125000				21.8			

*1000 psi = 6.895×10^6 Nm^{-2}.

with crystallites preferentially aligned with their *a*-axes parallel to the longitudinal fibre axis and with crystallite *c*-axes perpendicular to the fibre axis. The axial expansion of high modulus graphite fibres approaches the *a*-direction expansion of single crystal graphite, with values of $\alpha = -15 \times 10^{-7}°C^{-1}$ from 0 to 150°C, $\alpha = 0$ at approximately 400°C, and $\alpha = 9 \times 10^{-7}°C^{-1}$ from 600 to 800°C [15-17]. The *c*-axis expansion coefficient averages about $280 \times 10^{-7}°C$ from 0 to 1000°C [16], and is presumed to be similar to the radial expansion coefficient of the fibre.

During cooling from the hot-pressing temperature, the ceramic matrix becomes rigid and the graphite fibres tend to contract away from the surrounding matrix due to the relatively large radial expansion coefficient of the fibres. This would eliminate fibre-matrix interfacial contact and prevent the property increases observed for the composites. It therefore appears necessary to postulate chemical or mechanical bond formation between the fibre and matrix, in spite of the inability to observe evidence of this interfacial bonding by electron microscopy. The relative similarity between the axial thermal expansion coefficient of the fibres and that of the matrix precludes the development of substantial residual stresses during cooling from the hot-pressing temperature. However, the high radial thermal expansion coefficient of the fibres relative to the matrix will produce compressive stresses in the matrix during cooling, and place the interface in tension. The bending-over in the first load versus deflection curve on cycling, Fig. 7, was probably caused by matrix cracking at a higher strain than that at failure in an unreinforced body. This increase in matrix strain at failure is caused by the residual compressive stresses in the matrix. The fibre-matrix interfacial tensile stresses constitute a weakening of the fibre-matrix bond. The overall effect is a low interfacial shear strength and an increased matrix strength, with load transfer to the fibres occurring through the fibre-matrix bond. The low interfacial shear strength accounts for the low short-beam shear strengths observed, Table VII, and for transverse modulus of rupture values for composites which were lower than for the unreinforced compositions. The fibre-matrix interfacial tensile stresses also produced crack deflection and fibre pull-out, resulting in extremely high impact energies. Uninterrupted catastrophic crack propagation was inhibited by weak fibre-matrix interfacial bonds. It has been shown that the tensile stress component preceding a crack front may cause a weak interface to open up ahead of the crack front, diverting or inhibiting crack propagation [13]. Fibrous reinforcement tends to restrict crack length to interfibre distances and restrict separation of crack surfaces, where transverse fibres bridge the crack, thereby limiting crack growth. The unusually high impact energies observed for this composite system are due, in part, to the high modulus of rupture and relatively low modulus of elasticity coupled with fibre pull-out and crack deflection due to weak fibre-matrix bonding. The impact strength may be improved further by optimizing the fibre loading in the composite or possibly by using fibres having different mechanical properties.

The thermal expansion mismatch in $Li_2O \cdot Al_2O_3 \cdot 3SiO_2$ composites is apparently excessive, leading to a decline in properties. However, another factor which had a major effect on property variations is hot-pressing at the matrix melting point. Relatively high temperatures were found necessary to produce rapid densification and to obtain high density bodies with intimate fibre-matrix contact. Partial melting of the ceramic matrix produced a glassy phase which allowed this to occur. However, the low viscosity glass formed from $Li_2O \cdot Al_2O_3 \cdot nSiO_2$, where $n = 3$ and 4, caused extrusion in the mould and made processing control more difficult. Control of porosity and matrix vol % was poor, and these can vary on a local level within each body. This problem is almost non-existent for the highly viscous glass formed from $Li_2O \cdot Al_2O_3 \cdot 8SiO_2$. The presence of glass limits the upper use temperature of these composites [11]. The effects of residual glass on thermal expansion relationships, anisotropy of individual matrix grains, and the effect of graphite fibres on glass recrystallization have not yet been determined. The modulus of rupture for the various composites follows the reverse trend found for unreinforced bodies, being highest for $Li_2O \cdot Al_2O_3 \cdot 8SiO_2$, lower for $Li_2O \cdot Al_2O_3 \cdot 4SiO_2$ and lowest for $Li_2O \cdot Al_2O_3 \cdot 3SiO_2$ (high porosity lowered strength).

HM-S graphite fibres manufactured more recently resulted in composites of substantially lower properties. Composites fabricated using HM untreated fibres have shown marked increases in properties, with modulus of rupture values about 160 to 170 $\times 10^3$ psi (11.0×10^8

to 11.7×10^8 Nm^{-2}). It now appears that the particular type of proprietary surface treatment employed by the fibre manufacturer leaves residual impurities on the fibre surface. This causes moderate to severe property degradation by interfering with the thermal expansion relationships and/or interfacial bonding and depends on changes in the surface treatment process.

4. Summary and conclusions

A method has been developed for fabricating ceramic composites containing a high volume fraction of unidirectionally aligned graphite fibres in a dense and continuous lithium aluminosilicate matrix. Graphite fibre ceramic/matrix tapes are produced in a drum winding operation and subsequently hot-pressed into final form. This sytem possesses an unusual combination of properties including high strength, low density, excellent thermal shock resistance and outstanding impact resistance. The compounds $Li_2O{\cdot}Al_2O_3{\cdot}nSiO_2$, where $n = 3, 4$, and 8 may all be effectively utilized as matrices reinforced by graphite fibres. Substantial increases in modulus of rupture and modulus of elasticity have been obtained for all three matrix compositions reinforced by Hercules HM-S continuous graphite tows. Composites are generally characterized by low porosity, intimate fibre-matrix contact and an uncracked matrix, which is a result of a suitable thermal expansion match between fibre and matrix and the formation of a fibre-matrix bond. No strength loss is detected after five thermal shock cycles between room temperature and 1200°C. Izod impact energies of 20 to 30 ft lb in^{-2} (4.2×10^4 to 6.3×10^4 Jm^{2-}) (notched) and 75 ft lb in^{-2} 1.6×10^5 J in^{-2}) (unnotched) have been measured and are substantially higher than reported for most ceramic materials. Both graphite fibres and lithium aluminosilicates are commercially available and this system serves as both an extremely useful model system for study and as a practical system for product development. Tremendous design capability is inherent in this composite system both from the point of view of altering fibre volume, properties and orientation as well as controlling matrix composition.

Acknowledgements

The author expresses his appreciation to Mr D. Demyan for experimental work, Dr D. L. Gibbon and Mr J. Smith for optical and electron microscopy, Dr Y. Baskin, Dr V. Mimeault, Mr A. Pallozzi and Mr D. Beal for valuable technical discussions and assistance and Mr L. Staikoff for the scanning electron microscope picture.

References

1. M. W. LINDLEY and D. J. GODFREY, *Nature* **229** (1971) 192.
2. D. A. EVEREST and A. KELLY, 5th International Materials Symposium (University of California, Berkeley, 1971).
3. I. C. VISCONTI and G. A. COOPER, *Nature* **221** (1969) 754.
4. A. KELLY, "Strong Solids" (Oxford University Press, 1966).
5. R. A. PLENTY, Tech. Rept. AFML-TR-66-356, Part III (1969).
6. J. J. KROCHMAL, Tech. Rept. AFML-TR-67-207 (1967).
7. G. A. GRAVES, JUN, C. T. LYNCH, and K. S. MAZDIYASNI, *Bull. Amer. Ceram. Soc.* **49** (1970) 797.
8. L. H. VAN VLACK, "Elements of Materials Science" (Addison-Wesley, 1964).
9. R. A. HATCH, *Amer. Minerol.* **28** (1943) 471.
10. R. ROY and E. F. OSBORN, *J. Amer. Ceram. Soc.* **71** (1949) 2086.
11. S. R. LEVITT (submitted to *J. Amer. Ceram. Soc.*).
12. S. R. LEVITT and D. F. GIBBONS (in progress).
13. J. COOK and J. E. GORDON, *Proc. Roy. Soc.* **A282** (1964) 508.
14. F. A. HUMMEL, US Patent Re-24795 (1960).
15. R. BACON, AFML-TR-66-334, Part II, December 1967.
16. J. B. NELSON and D. P. REILLY, *Phys. Soc. Proc.* **57** (1945) 477.
17. B. BUTLER, S. DUBERE, and J. TIDMORE, Tenth Biennial Conference on Carbon, Bethlehem, Pennsylvania (1971).

Received 3 July and accepted 19 November 1972.